

Search for a Dark-Matter-Induced Cosmic Axion Background with ADMX

T. Nitta^{1,*}, T. Braine¹, N. Du¹, M. Guzzetti¹, C. Hanretty¹, G. Leum¹, L. J. Rosenberg¹, G. Rybka¹, J. Sinnis¹, John Clarke², I. Siddiqi², M. H. Awida³, A. S. Chou³, M. Hollister³, S. Knirck³, A. Sonnenschein³, W. Wester³, J. R. Gleason⁴, A. T. Hipp⁴, P. Sikivie⁴, N. S. Sullivan⁴, D. B. Tanner⁴, R. Khatiwada^{5,3}, G. Carosi⁶, N. Robertson⁶, L. D. Duffy⁷, C. Boutan⁸, E. Lentz⁸, N. S. Oblath⁸, M. S. Taubman⁸, J. Yang⁸, E. J. Daw⁹, M. G. Perry⁹, C. Bartram¹⁰, J. H. Buckley¹¹, C. Gaikwad¹¹, J. Hoffman¹¹, K. W. Murch¹¹, M. Goryachev¹², E. Hartman¹², B. T. McAllister^{12,13}, A. Quiskamp¹², C. Thomson¹² and M. E. Tobar¹²

(ADMX Collaboration)

J. A. Dror¹⁴, H. Murayama^{2,15,16} and N. L. Rodd¹⁷¹University of Washington, Seattle, Washington 98195, USA²University of California, Berkeley, California 94720, USA³Fermi National Accelerator Laboratory, Batavia, Illinois 60510, USA⁴University of Florida, Gainesville, Florida 32611, USA⁵Illinois Institute of Technology, Chicago, Illinois 60616, USA⁶Lawrence Livermore National Laboratory, Livermore, California 94550, USA⁷Los Alamos National Laboratory, Los Alamos, New Mexico 87545, USA⁸Pacific Northwest National Laboratory, Richland, Washington 99354, USA⁹University of Sheffield, Sheffield S10 2TN, United Kingdom¹⁰Stanford Linear Accelerator Center, Menlo Park, California 94025, USA¹¹Washington University, St. Louis, Missouri 63130, USA¹²University of Western Australia, Perth, Western Australia 6009, Australia¹³Swinburne University of Technology, Melbourne, Victoria 3122, Australia¹⁴Santa Cruz Institute for Particle Physics and Department of Physics, University of California, 1156 High St, Santa Cruz, California 95060, USA¹⁵Lawrence Berkeley National Laboratory, Berkeley, California 94720, USA¹⁶Kavli Institute for the Physics and Mathematics of the Universe (WPI), The University of Tokyo, Kashiwa 277-8583, Japan¹⁷Theoretical Physics Department, CERN, 1 Esplanade des Particules, CH-1211 Geneva 23, Switzerland (Received 19 March 2023; revised 5 June 2023; accepted 16 August 2023; published 8 September 2023)

We report the first result of a direct search for a cosmic *axion* background (*CaB*)—a relativistic background of axions that is not dark matter—performed with the axion haloscope, the Axion Dark Matter eXperiment (ADMX). Conventional haloscope analyses search for a signal with a narrow bandwidth, as predicted for dark matter, whereas the *CaB* will be broad. We introduce a novel analysis strategy, which searches for a *CaB* induced daily modulation in the power measured by the haloscope. Using this, we repurpose data collected to search for dark matter to set a limit on the axion photon coupling of a *CaB* originating from dark matter cascade decay via a mediator in the 800–995 MHz frequency range. We find that the present sensitivity is limited by fluctuations in the cavity readout as the instrument scans across dark matter masses. Nevertheless, we suggest that these challenges can be surmounted using superconducting qubits as single photon counters, and allow ADMX to operate as a telescope searching for axions emerging from the decay of dark matter. The daily modulation analysis technique we introduce can be deployed for various broadband rf signals, such as other forms of a *CaB* or even high-frequency gravitational waves.

DOI: [10.1103/PhysRevLett.131.101002](https://doi.org/10.1103/PhysRevLett.131.101002)

Published by the American Physical Society under the terms of the [Creative Commons Attribution 4.0 International license](https://creativecommons.org/licenses/by/4.0/). Further distribution of this work must maintain attribution to the author(s) and the published article's title, journal citation, and DOI. Funded by SCOAP³.

Axions, originally motivated by their simple solution to the strong *CP* problem [1–4], have since been accepted more broadly as a compelling extension of the standard model. Most searches for axions that are relics of the early

Universe assume they make up a local nonrelativistic fluid, which is characteristic of dark matter [5–7]. However, a local axion energy density could take on other forms. Axions could be produced in the early Universe thermally, via parametric resonance, the decay of topological defects, or alternatively could emerge in the late Universe from the decay of another dark matter candidate [8]. Collectively, the relativistic abundance of such axions would form a cosmic *axion* background (CaB): an axion analog of the photons in the cosmic microwave background. The CaB, if produced in the early Universe, would constitute a form of dark radiation and therefore a contribution to ΔN_{eff} , which CMB-S4 will be well placed to detect [9] (and in fact, there may even be a mild hint for from the Hubble tension [10,11]). In the late Universe, the CaB will constitute a local axion energy density, analogous to axion dark matter, and therefore can be searched for with axion haloscopes [12–26]. The principal difference, however, is that whereas dark matter is narrow spectrally, the CaB can be comparatively very broad. In a ~ 1 GHz frequency range, dark matter has a bandwidth of $\mathcal{O}(1$ kHz), whereas the CaB bandwidth could be $\mathcal{O}(100$ MHz) or larger.

In this work, we perform the first direct search for the CaB with the Axion Dark Matter eXperiment (ADMX) [27–33], and therefore provide a direct search for additional dark radiation. To do so, we focus on one specific form the CaB could take: relativistic axions, a , emerging from the decay of dark matter particles, χ . The search can therefore be considered as an extension of the dark matter indirect detection program, with axions acting as final states. As we will review, this signal gives rise to power in a resonant cavity that modulates over the course of a day. Accordingly, we introduce an analysis strategy to directly search for modulating power in an existing ADMX dataset, and in this way construct the first analysis for the CaB [34].

ADMX as a telescope for dark matter decay.—We begin by outlining the details of the model we consider and the power it could generate in ADMX. We search for the axions arising from the decay of dark matter. The simplest realization of such a scenario would appear to be a two-body decay, $\chi \rightarrow aa$. However, as discussed in Ref. [8], axions are bosons so that such a decay can be enormously Bose enhanced, which would lead to a runaway decay and rapidly deplete the dark matter. The runaway would not occur if the decay is slightly modified, for instance, by the inclusion of an intermediate state φ in a cascade decay. For this reason, we focus on axions arising from the decay channel $\chi \rightarrow \varphi\varphi \rightarrow aaaa$. In general, the spectrum of axions produced in the decays will depend on m_{DM} , m_φ , and m_a . As we focus on relativistic axions, we always assume m_a is negligible. If we further assume $m_\varphi \ll m_{\text{DM}}$, then the spectrum of axions depends on two parameters: m_{DM} and the dark matter lifetime, τ (see, e.g., Refs. [36,37]). We emphasize that our focus here is on studying scenarios that realize these kinematics; there will

be a variety of models in which such a cascade scenario could arise. In the Supplemental Material [38] we provide an explicit example that realizes these kinematics: a cubic dark matter-mediator interaction and a quadratic axion derivative coupling to the mediator. While there is no dedicated experimental search of this scenario, there are constraints on the lifetime for dark matter to decay into a relativistic species, for instance, dark energy survey (DES) measurements require at 95% confidence limits (C.L.) $\tau > 25$ Gyr $\sim 1.8t_{\text{U}}$ [41], where t_{U} is the present age of the Universe [42]. We expect this to reasonably approximate the bound on the lifetime when the fraction of dark matter which decayed is small and the lifetime of any intermediate particle is negligible compared to the age of the Universe.

As detailed in the Supplemental Material [38], the resulting CaB from the dark matter decays will generate the following differential power in a resonant cavity,

$$\begin{aligned} \frac{dP_a}{d\omega}(\omega, \alpha) = & \frac{\rho_c g_{a\gamma\gamma}^2 B^2 V C \beta}{8Q((\omega - \omega_0)^2 + (\omega_0/2Q)^2)} \frac{\omega_0^3}{\omega^3} \\ & \times \left[\Omega_a^{\text{MW}}(\omega) \int dz d\phi \mathcal{D}_\nu(-z) K(\omega, \alpha) \right. \\ & \left. + \frac{1}{2} \Omega_a^{\text{EG}}(\omega) \int dz d\phi K(\omega, \alpha) \right]. \quad (1) \end{aligned}$$

The power depends on properties of the cavity and of the axion. For the cavity, B is the external magnetic field, V is its volume, Q is the quality factor, β is the coupling between the cavity and antenna, C is the cavity form factor for the TM_{010} mode [33], and ω_0 is the resonant angular frequency of the same mode. For the axion, we have the axion energy ω and the expressions in parentheses detail the flux of axions arising from decays within the Milky Way (MW) and extragalactic (EG) decays. The full expressions for the flux are given in the Supplemental Material [38], but briefly, $\Omega_a(\omega)$ describes the spectrum of axions and depends on the lifetime τ , vanishing as $\tau \rightarrow \infty$, whereas the angular distributions are controlled by the integrands. Specifically, we integrate over the full sky using spherical coordinates ϕ and $\theta = \arccos z$. The parameter $\mathcal{D}_\nu(z)$ describes the angular dependence of decays in the MW, which occur primarily at the Galactic Center, and there is no analog for the EG flux as the flux of axions is essentially isotropic. The normalization factor, $\rho_c \simeq 4.8$ keV/cm³, denotes the critical density.

The final ingredient in Eq. (1), $K(\omega, \alpha)$, generates the daily modulation, and describes the fact that the relativistic axion is not spatially coherent across the instrument. As the ADMX cavity is not a sphere, the coherence across the cavity will depend on α , the angle between the axion, $\hat{\mathbf{k}}$, and the magnetic field, $\hat{\mathbf{z}}$. For an ideal cylindrical cavity of height L and radius R , we can compute [8]

$$K(\omega, \alpha) = \left[\frac{\sin(\omega L \cos \alpha)}{\omega L \cos \alpha} \frac{J_0(\omega R \sin \alpha)}{1 - (\omega R \sin \alpha / j_{01})^2} \right]^2, \quad (2)$$

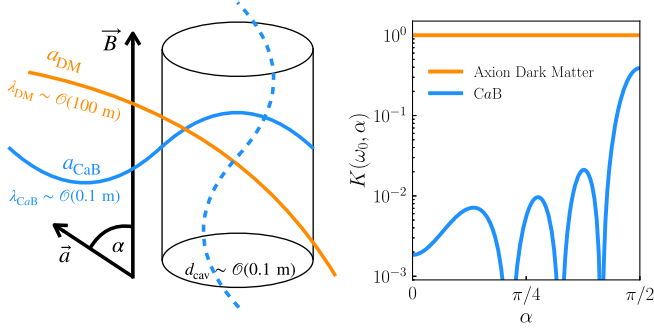


FIG. 1. Left: a schematic depiction of the spatial coherent length of a dark matter [$\lambda_{\text{DM}} \sim \mathcal{O}(100 \text{ m})$, orange] or CaB [$\lambda_{\text{CaB}} \sim \mathcal{O}(0.1 \text{ m})$, light blue] signal over the TM_{010} mode of a cylindrical cavity [$d_{\text{cav}} \sim \mathcal{O}(0.1 \text{ m})$, black cylinder]. The dark matter signal is coherent across the cavity, and therefore independent of the incident direction, whereas the CaB is not, and therefore the dashed and solid curves can give rise to significantly different signals. Right: a quantification of this effect using the expression in Eq. (2), where α is the angle between the incident axion and the cavity magnetic field, $R = 0.2 \text{ m}$, and $L = 1 \text{ m}$. The power of photons converted from the CaB is maximized at $\alpha = \pi/2$, when the cavity magnetic field is perpendicular to the incident axions, and suppressed when $\alpha = 0$.

where J_0 is a Bessel function of the first kind, and j_{01} is that function's first zero. A depiction of why this factor arises for the CaB , but not dark matter, is given in Fig. 1. Axion dark matter (orange) has a significantly larger de Broglie wavelength than its Compton wavelength. Consequently, it sources a spatially coherent effect across the cavity. This is not the case for the CaB (light blue), which has a de Broglie wavelength comparable to its Compton wavelength and therefore can oscillate spatially across the cavity. The effect of the resulting interference is described by $K(\omega, \alpha)$. While this factor suppresses the overall power [$K(\omega, \alpha) \leq 1$], the way in which it does so is critically dependent on the incident angle of the wave—for instance, a wave incident down the height of the cavity will oscillate many more times than one incident radially, given that $L \gg R$. Combining this effect with the fact that the axions originate from dark matter decays in the MW arise preferentially from the Galactic Center and that cavity magnetic field orientation will rotate with the Earth throughout the day, results in a unique daily modulation signal that we will exploit to search for the CaB [43].

A daily modulation analysis.—Having defined the signal, we now outline the analysis we intend to perform on existing ADMX data, which will fundamentally make use of the daily modulation emerging from $K(\omega, \alpha)$. Briefly, ADMX uses an axion haloscope designed to search for axions that could constitute the local dark matter halo using a cold resonant cavity immersed in a static magnetic field. The apparatus consists of a 136ℓ cylindrical copper-plated stainless steel microwave cavity surrounded by a 7.5 T superconducting magnet. The resonant frequency of the

cavity is adjusted through the use of two movable internal bulk copper rods. The rf power in the cavity is extracted using an antenna, and then amplified with a Josephson parametric amplifier (JPA) [47] and the following heterostructure field effect transistor (HFET) amplifiers [48]. For further details, see Ref. [49].

In the present work, we will search for a CaB signal in existing ADMX data that were collected with the explicit purpose of searching for axion dark matter. The dataset amounts to a series of power measurements taken over 100-sec intervals throughout the day, each taken at different resonant frequencies, and scanned in search of the unknown dark matter mass. For each of these measurements, a dark matter signal would emerge as a narrow line in the data on top of a broad thermal photon background. There is then a relatively clean separation into frequency regions where there is background only and those where there is signal and background, which allows one to calibrate the signal strength with respect to the thermal noise within one digitization bandwidth. Such a separation is not possible for the CaB . The signal is broader than both the cavity linewidth and the digitization bandwidth: the only way to distinguish a CaB signal from the thermal background in a single scan would be to exploit the B^2 scaling in Eq. (1). If we combine multiple scans taken throughout the day, however, we can search for the daily modulation of the CaB signal. Unfortunately, the backgrounds also vary with time; there is time variation in the gain as well as temperature drifts in the system which are mentioned later. The HFET response is relatively stable, about 2% of fluctuation through a week, and therefore we did not apply any calibration, we rather add the fluctuation as systematic uncertainty as shown later. The bias current of the JPA is adjusted every four digitizations to maximize the dark matter signal-to-noise ratio. During this process, gain stability is not the figure of merit, and the gain can vary between 15 and 30 dB. This will lead to large fluctuations in the observed power as a function of time, and will form an important background when searching for a modulating signal.

To mitigate the impact of gain fluctuations, we define a new observable, which we refer to as the power excess modulation (PEM),

$$\text{PEM} = \frac{\bar{P}(t)/G_{\text{JPA}}(t) - \langle \bar{P}(t)/G_{\text{JPA}}(t) \rangle}{\langle \sigma_P(t)/G_{\text{JPA}}(t) \rangle} k_B T_{\text{sys}} \sqrt{\frac{b}{T}}. \quad (3)$$

Here, $\bar{P}(t)$ and $\sigma_P(t)$ are the mean and standard deviation of the power in a dataset collected at a time t , computed over the frequencies in the digitization bandwidth, which is 100 Hz for the data we used. For that same dataset, we further use the gain in the JPA, denoted by $G_{\text{JPA}}(t)$. Finally, $\langle \cdot \rangle$ corresponds to expressions averaged over a full day, T_{sys} is the system-noise temperature, typically around 500 mK, k_B is the Boltzmann constant, b is the bin width

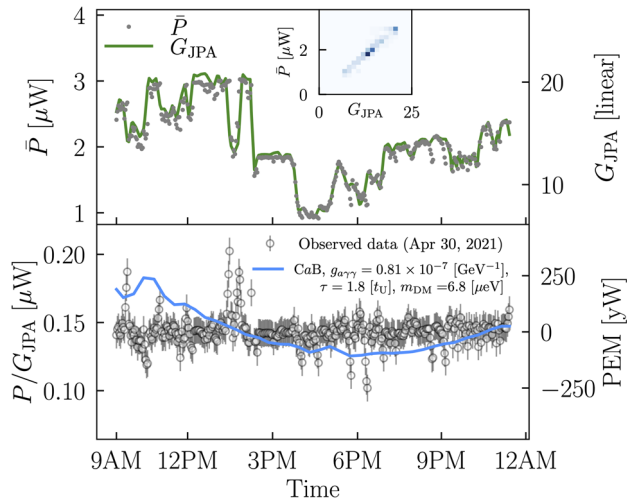


FIG. 2. Top: an example of the mean power (gray) as a function of time collected on April 30, 2021. We further show the JPA gain in green, and in the inset demonstrate the two are strongly correlated. Bottom: For the same dataset, we divide the mean power out by the gain (left axis) and show the resulting PEM computed according to Eq. (3) (right axis, gray circle). The light blue line shows CaB PEM as a reference. Parameters are chosen to be visible in this scale. A peak of P/G_{JPA} at around 1–2 PM is due to the gain instability of the JPA caused by the liquid helium refill of the ADMX reservoir.

of the spectrum, and T is the collection time for the dataset, which for the results we use is 100 sec.

The PEM in Eq. (3) quantifies the variation of the power in a single scan relative to the average for that day, accounting for the measured gain. If we have PEM values collected at a series of times t_i , we can combine these into a single dataset $d_{\text{PEM}} \equiv \{\text{PEM}(t_i)\}$, within which we can look for an axion signal oscillating throughout the day. To provide an example of the data, in Fig. 2 (top) we show the mean power as a function of time throughout the day, for data taken on April 30, 2021. As can be seen, the gain from the JPA varies by an $\mathcal{O}(1)$ value throughout the day, and those fluctuations are strongly correlated with the observed value of \bar{P} . In the bottom panel, we show the power after the gain has been divided out, and it is within this data we search for a signal of the CaB, which is also shown. We note that the use of $\bar{P}(t)/G_{\text{JPA}}(t)$ rather than the average power greatly improves the sensitivity to the CaB. Nevertheless, our knowledge of $G_{\text{JPA}}(t)$ is imperfect. Since measurements of the JPA gain were only performed approximately every 5 min, meaning values are not available for every dataset. Therefore, residual variations caused by the JPA were taken into account as a systematic uncertainty described later.

Data reduction and systematics.—We now describe the existing ADMX data we will use to search for the CaB. In particular, we made use of an existing ADMX search for dark matter performed over the frequency range 800–1020 MHz [33]. Given the background considerations are different

when searching for the CaB rather than dark matter, we applied additional quality cuts to the dataset. First, the JPA gain was found to be significantly unstable during the time when the data in the 995–1020 MHz frequency range were collected, and, consequently, we decided to exclude this entirely. Second, we discarded all rescan datasets—measurements performed to follow up any potential candidates observed in the dark matter search—to avoid discontinuities in the PEM. Even though these could be accounted for, the amount of rescan data is negligible, so including it would not substantially improve our sensitivity. Finally, we discarded those datasets which were collected while the liquid helium was being refilled, as the vibrations led to further fluctuations in the JPA gain. These three cuts reduced our initial dataset by roughly 50%.

Before analyzing the data, there are three sources of systematic uncertainty we identified that are beyond those conventionally accounted for in haloscope analyses [50], as they are unique to the PEM analysis: short timescale fluctuations dominated by the JPA variation, power fluctuations from the other parts of the radio frequency (rf) system, and an imperfect calculation of $K(\omega, \alpha)$. We describe each of these below in turn.

To begin with, as mentioned the $\bar{P}(t)$ values we measure are collected every ~ 100 sec, whereas JPA gain variation are only remeasured every ~ 5 min. The two are strongly correlated, however, as clearly shown in Fig. 2, and therefore the imperfect knowledge of G_{JPA} represents an uncertainty to be accounted for. The gain fluctuations are statistically random and approximately Gaussian. In order to model the systematic error induced by these fluctuations, we take the full PEM dataset as a function of time and fit it with a Savitzky-Golay (SG) filter (length 201 and polynomial order 3). The SG filter is used to remove all fluctuations over timescales larger than ~ 5 min, for instance, a potential HFET gain drift or even a possible contribution from the CaB. The remaining short-time fluctuations are attributed to the JPA, and we model these as a Gaussian with a width determined by the standard deviation of these residuals. This fluctuation is then combined with the other systematic uncertainties we account for in quadrature. We emphasize that the SG filter is used only for estimating the uncertainty; the fit to search for a CaB amplitude is performed without the SG filter.

While variations in the JPA gain are the dominant source of temporal variations in the power, there are other milder contributions from the rf system, such as variations in temperature, although the leading second-order effect is gain fluctuations in the HFET. This uncertainty was estimated by directly measuring the stability of the room-temperature rf system. During the measurements, the part of the rf system that is cooled down was disconnected from the full apparatus, so that the fluctuations were only measured in the latter. Through this process, the fluctuations were measured to be at most 2%, and this value was

incorporated as a systematic uncertainty. There is, however, an additional HFET amplifier in the part of the instrument that is cooled. Therefore, we disconnected it from the above measurement, and we conservatively assign the same 2% uncertainty to the additional HFET amplifier. Combining the two in quadrature, we then attribute the full rf system (excluding the JPA) a systematic uncertainty of 2.8%.

The final source of systematic uncertainty arises from the calculation of $K(\omega, \alpha)$. We determined this from Eq. (2) though that result assumes a perfectly cylindrical cavity. For comparison, the relevant form factor for dark matter, C , deviates from this perfect value due to the presence of the tuning rods in the cavity, for example, and is precisely determined using simulations with Ansys HFSS. We attribute an uncertainty of 30% to our computation of K , as this is the magnitude of the variation in C as the tuning rods are moved confirmed by simulation with Ansys HFSS.

A CaB search in existing ADMX data.—Having described our dataset, d_{PEM} , and the PEM analysis framework, we turn to the search for the CaB. We will perform the search using a Gaussian likelihood analysis, determining limits with a likelihood ratio test statistic. While we expect fluctuations in the power throughout the day from various background sources as described above, these have been accounted for either by our explicit inclusion of G_{JPA} in the PEM or else through the use of systematic uncertainties. Accordingly, our null hypothesis (H_0) is simply that $\text{PEM} = 0$. For our alternative hypothesis (H_1) we add to the null hypothesis a contribution from the CaB. As a reference point, we consider the largest CaB signal that can be presently obtained: this occurs when we take $\tau = 1.8t_U$, and $g_{a\gamma\gamma}^{\text{CAST}} = 0.66 \times 10^{-10} \text{ GeV}^{-1}$, i.e., saturating the DES and CAST 95% confidence limits, respectively (with the latter taken from Ref. [51]). From this maximally allowed hypothesis we can then vary $g_{a\gamma\gamma}$, which varies the overall amplitude of the signal according to Eq. (1), determine the best fit value and then define a signal strength $\mu = (g_{a\gamma\gamma}^{\text{fit}}/g_{a\gamma\gamma}^{\text{CAST}})^2$, which will also be the ratio of the best fit PEM to that predicted when $\mu = 1$. Note we choose to vary $g_{a\gamma\gamma}$ rather than τ , as the former solely scales the signal amplitude; the lifetime changes the shape of the signal as we describe in the Supplemental Material [38]. From here we define a signal hypothesis H_1 as the alternative hypothesis where μ obtains its preferred value in the data.

From these hypotheses, we define the probability of H_0 and H_1 as $p(H_0)$ and $p(H_1)$, respectively. We then set the following criteria: (i) $p(H_0) > 0.003$: no evidence for new physics; (ii) $p(H_0) < 0.003$ and $p(H_1) < 0.003$: the null hypothesis is disfavored, but there is no evidence for the CaB; and (iii) $p(H_0) < 0.003$ and $p(H_1) > 0.003$: there is a preference for the CaB. In the above, 0.003 corresponds to the 3σ threshold. In the absence of evidence for the maximal CaB signal predicted by H_1 , we can determine a 95% confidence level (CL) limit on $g_{a\gamma\gamma}$ by scaling $g_{a\gamma\gamma}^{\text{CAST}}$ with $\sqrt{\mu} + 1.644 \times \Delta\mu$, where $\Delta\mu$ is fit uncertainty on the

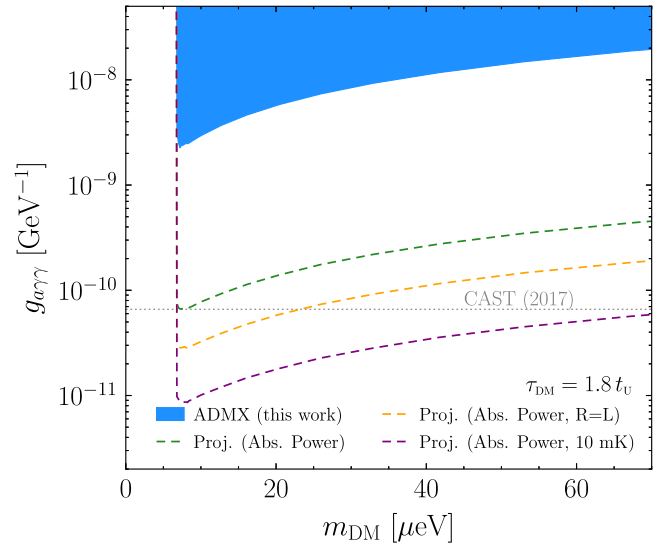


FIG. 3. 95% C.L. on $g_{a\gamma\gamma}$ for a CaB arising from the decay of dark matter, assuming $\tau = 1.8t_U$. The horizontal dashed line shows the CAST bound [51] which assumes general axion-photon coupling from axion production in the Sun. The results do not yet exceed the CAST bound, and are primarily limited by fluctuations in the JPA gain. These would be removed if the same analysis were performed using an absolute power measurement, and with other improvements such as a reduced system temperature or modified cavity geometry, significantly enhanced sensitivity can be achieved. See text for details.

best fit value of μ . The value of 1.644 arises from 95% of the one-sided Gaussian probability.

Using the above procedure, we searched for a signal of the CaB between 800 and 995 MHz, which in total amounted to 143 days of data. Nevertheless, we found that the data taken near 850 MHz dominated the sensitivity as it was taken over a period of time where the JPA was especially stable. We analyzed each day of data separately and found that all spectra were consistent with the expected background in the absence of a CaB, i.e., $p(H_0) > 0.003$. Therefore, we use the combined data over all days to establish an upper limit on $g_{a\gamma\gamma}$. The results are shown in Fig. 3 with $\tau = 1.8t_U$; results for larger values of τ , for which our constraints on $g_{a\gamma\gamma}$ degrade, are provided in the Supplemental Material [38].

At present, this first search for the CaB is not able to reach the allowed parameter space below $g_{a\gamma\gamma}^{\text{CAST}}$. The primary limitation is that existing haloscopes are only sensitive to the relative power excess, for instance, as encapsulated in the PEM. However, this is not a fundamental limitation. For example, a single photon counter using a superconducting qubit (see, e.g., Ref. [52]) essentially measures the absolute photon occupation number in the cavity, which would allow for absolute power measurements. In this case, thermal excitation or false positive rate of qubits dictates the background level. Such a measurement would remove the need to subtract the mean,

as we do in the PEM given we are presently only sensitive to time variations rather than the absolute scale. As a result, at present we are completely insensitive to the contribution to the CaB from extragalactic decays, worsening the sensitivity to $g_{\gamma\gamma}$ by $\sim 2/5$. An additional benefit of an absolute power measurement is that as it only measures the number of states in the cavity it will render the amplifiers gain fluctuations negligible when at present they are our dominant background. Removing this background would improve our sensitivity to roughly $g_{\gamma\gamma}^{CAST}$. In addition to measuring the absolute power, single photon counters using a superconducting qubit can potentially achieve a noise temperature of around 10 mK by using quantum nondemolition measurements [53], which would improve the sensitivity further. Finally, as we describe in the Supplemental Material [38], the ADMX cavity geometry ($L \sim 5R$) significantly suppresses the CaB power through $K(\omega_0, \alpha)$. A cavity with $L \sim R$ would largely lift that suppression. In Fig. 3 we show the expected improved sensitivity that would result from each of these considerations.

Discussion.—We have performed the first direct search for the CaB with an axion haloscope. While there are many forms the CaB could take, we focused on the possibility of a cascade decay of dark matter to axions, $\chi \rightarrow \varphi\varphi \rightarrow aaaa$, and exploited the resulting daily modulation in the signal. In particular, we introduced the PEM analysis to search for a daily variation in the power, and then applied this method to existing ADMX data.

While our results are specific to the dark matter decay CaB , the methodology employed here is general and can be used to search for other possible broadband signals in axion haloscopes. The present sensitivity we obtained with the PEM is roughly an order of magnitude weaker than might have been expected, and this was solely due to the large variations in the gain. To improve on this, future measurements can monitor the relative HFET gain fluctuation, for instance, by injecting rf tones during data taking and thereby have an accurate measurement of the gain at all times rather than every 5 min. Also, data taking without fine-tuning of the JPA bias current at the same cavity resonant frequency would realize stabler PEM spectra. Separately, looking even further forward, the sensitivity will improve significantly once absolute power measurements in the cavity are possible, an avenue that will be opened by single photon measurements. Combining this improvement with the expected strides axion haloscopes will make in the coming decade, it is likely this will be only the first of many searches for nondark matter signals with such instruments. Indeed, it could well be that the first signs of new physics in these instruments emerges in the form of a CaB , high-frequency gravitational waves (see, e.g., Refs. [54,55]), or another as yet unanticipated signal.

The work presented benefited from discussions with members of the HAYSTAC Collaboration, in particular,

Maryam H. Esmat, Sumita Ghosh, Alexander F. Leder, and Danielle Speller. This work was supported by the U.S. Department of Energy through Grants No. DE-SC0009800, No. DESC0009723, No. DE-SC0010296, No. DE-SC0010280, No. DE-SC0011665, No. DEFG02-97ER41029, No. DEFG02-96ER40956, No. DEC03-76SF00098, and No. DE-SC0017987. Fermilab is a U.S. Department of Energy, Office of Science, HEP User Facility. Fermilab is managed by Fermi Research Alliance, LLC (FRA), acting under Contract No. DE-AC02-07CH11359. Additional support was provided by the Heising-Simons Foundation and by the Lawrence Livermore National Laboratory LDRD office. Pacific Northwest National Laboratory is a multiprogram national laboratory operated for the U.S. DOE by Battelle Memorial Institute under Contract No. DE-AC05-76RL01830. Prepared in part by LLNL under Contract No. DE-AC52-07NA27344, Release No. LLNL-JRNL-845987". T.N. is supported by JSPS Overseas Research Fellowships No. 202060305. C. Bartram acknowledges support from the Panofsky Fellowship at SLAC.

*Corresponding author: tnitta@icepp.s.u-tokyo.ac.jp

†Present address: International Center for Elementary Particle Physics (ICEPP), The University of Tokyo, Tokyo 113-0033, Japan.

- [1] R. D. Peccei and H. R. Quinn, *Phys. Rev. D* **16**, 1791 (1977).
- [2] S. Weinberg, *Phys. Rev. Lett.* **40**, 223 (1978).
- [3] R. D. Peccei and H. R. Quinn, *Phys. Rev. Lett.* **38**, 1440 (1977).
- [4] F. Wilczek, *Phys. Rev. Lett.* **40**, 279 (1978).
- [5] P. Sikivie, *Rev. Mod. Phys.* **93**, 015004 (2021).
- [6] A. Hook, *Proc. Sci.*, TASI2018 (2019) 004 [arXiv:1812.02669].
- [7] C. B. Adams, N. Aggarwal, A. Agrawal, R. Balafandiev, C. Bartram, M. Baryakhtar *et al.*, arXiv:2203.14923.
- [8] J. A. Dror, H. Murayama, and N. L. Rodd, *Phys. Rev. D* **103**, 115004 (2021).
- [9] K. N. Abazajian *et al.* (CMB-S4 Collaboration), arXiv:1610.02743.
- [10] D. Baumann, D. Green, and B. Wallisch, *Phys. Rev. Lett.* **117**, 171301 (2016).
- [11] L. Verde, T. Treu, and A. G. Riess, *Nat. Astron.* **3**, 891 (2019).
- [12] P. Sikivie, *Phys. Rev. Lett.* **51**, 1415 (1983).
- [13] J. L. Ouellet *et al.*, *Phys. Rev. D* **99**, 052012 (2019).
- [14] G. B. Gelmini, A. J. Millar, V. Takhistov, and E. Vitagliano, *Phys. Rev. D* **102**, 043003 (2020).
- [15] A. Arvanitaki and A. A. Geraci, *Phys. Rev. Lett.* **113**, 161801 (2014).
- [16] J. Liu, K. Dona, G. Hoshino, S. Knirck, N. Kurinsky, M. Malaker *et al.* (BREAD Collaboration), *Phys. Rev. Lett.* **128**, 131801 (2022).
- [17] D. Aybas, J. Adam, E. Blumenthal, A. V. Gramolin, D. Johnson, A. Kleyheeg, S. Afach *et al.*, *Phys. Rev. Lett.* **126**, 141802 (2021).

- [18] T. Wu, J. W. Blanchard, G. P. Centers, N. L. Figueroa, A. Garcon, P. W. Graham, Derek F. Jackson Kimball, S. Rajendran, Y. V. Stadnik, A. O. Sushkov, A. Wickenbrock, and D. Budker, *Phys. Rev. Lett.* **122**, 191302 (2019).
- [19] L. Brouwer *et al.*, *Phys. Rev. D* **106**, 112003 (2022).
- [20] C. P. Salemi *et al.*, *Phys. Rev. Lett.* **127**, 081801 (2021).
- [21] K. M. Backes *et al.*, *Nature (London)* **590**, 238 (2021).
- [22] M. Baryakhtar, J. Huang, and R. Lasenby, *Phys. Rev. D* **98**, 035006 (2018).
- [23] P. Brun *et al.* (MADMAX Collaboration), *Eur. Phys. J. C* **79**, 186 (2019).
- [24] A. V. Gramolin, D. Aybas, D. Johnson, J. Adam, and A. O. Sushkov, *Nat. Phys.* **17**, 79 (2021).
- [25] I. Irastorza *et al.* (IAXO Collaboration), *J. Cosmol. Astropart. Phys.* **06** (2011) 013.
- [26] M. Esmat and Haloscope At Yale Sensitive To Axion CDM (Haystac) Team, in APS April Meeting Abstracts, *APS Meeting Abstracts* (2022), Vol. 2022, p. S10.006, <https://meetings.aps.org/Meeting/APR22/Session/S10.6>.
- [27] S. Asztalos, E. Daw, H. Peng, L. J. Rosenberg, C. Hagmann, D. Kinion *et al.*, *Phys. Rev. D* **64**, 092003 (2001).
- [28] S. Asztalos, R. Bradley, L. Duffy, C. Hagmann, D. Kinion, D. Moltz *et al.*, *Phys. Rev. D* **69**, 011101(R) (2004).
- [29] S. J. Asztalos *et al.*, *Astrophys. J.* **571**, L27 (2002).
- [30] S. J. Asztalos *et al.*, *Phys. Rev. Lett.* **104**, 041301 (2010).
- [31] N. Du, N. Force, R. Khatiwada, E. Lentz, R. Ottens, L. J. Rosenberg *et al.* (ADMX Collaboration), *Phys. Rev. Lett.* **120**, 151301 (2018).
- [32] T. Braine, R. Cervantes, N. Crisosto, N. Du, S. Kimes, L. J. Rosenberg *et al.* (ADMX Collaboration), *Phys. Rev. Lett.* **124**, 101303 (2020).
- [33] C. Bartram *et al.* (ADMX Collaboration), *Phys. Rev. Lett.* **127**, 261803 (2021).
- [34] For an alternative detection scheme which exploits the upcoming Square Kilometer Array to search for photon signals originating from the conversion of relativistic axions in astrophysical magnetic fields, see Ref. [35].
- [35] A. Kar, T. Kumar, S. Roy, and J. Zupan, [arXiv:2212.04647](https://arxiv.org/abs/2212.04647).
- [36] G. Elor, N. L. Rodd, and T. R. Slatyer, *Phys. Rev. D* **91**, 103531 (2015).
- [37] G. Elor, N. L. Rodd, T. R. Slatyer, and W. Xue, *J. Cosmol. Astropart. Phys.* **06** (2016) 024.
- [38] See Supplemental Material at <http://link.aps.org/supplemental/10.1103/PhysRevLett.131.101002> for the detail of the flux of axions arising from decays within the Milky Way and extragalactic decays, which includes Refs. [39,40].
- [39] J. F. Navarro, C. S. Frenk, and S. D. M. White, *Astrophys. J.* **462**, 563 (1996).
- [40] J. F. Navarro, C. S. Frenk, and S. D. M. White, *Astrophys. J.* **490**, 493 (1997).
- [41] A. Chen *et al.*, *Phys. Rev. D* **103**, 123528 (2021).
- [42] To derive this value from Ref. [41], we set the ratio of the amount of dark matter converted into dark radiation divided by the amount of dark matter today, which we approximate by $(1 - e^{-t\nu/\tau})/e^{-t\nu/\tau}$, equal to their 95% C.L. limit on ζ , marginalized over all nuisance parameters (0.72).
- [43] We emphasize that the daily modulation signal we describe arises solely from the interaction of the CaB wave with the cavity. This can be contrasted with other possible modulating signals, such as that proposed for axion quark nugget dark matter, which generates a relativistic axion signal where the amplitude of the signal oscillates throughout the day, see Refs. [44–46].
- [44] H. Fischer, X. Liang, A. Zhitnitsky, Y. Semertzidis, and K. Zioutas, *Phys. Rev. D* **98**, 043013 (2018).
- [45] X. Liang, A. Mead, Md Shahriar Rahim Siddiqui, L. Van Waerbeke, and A. Zhitnitsky, *Phys. Rev. D* **101**, 043512 (2020).
- [46] D. Budker, V. V. Flambaum, X. Liang, and A. Zhitnitsky, *Phys. Rev. D* **101**, 043012 (2020).
- [47] I. Siddiqi, R. Vijay, F. Pierre, C. M. Wilson, M. Metcalfe, C. Rigetti, L. Frunzio, and M. H. Devoret, *Phys. Rev. Lett.* **93**, 207002 (2004).
- [48] L. N. Factory, 0.6–2 ghz cryogenic low noise amplifier, https://www.lownoisefactory.com/files/1215/2585/7504/LNF-LNC0.6_2A.pdf.
- [49] R. Khatiwada *et al.*, *Rev. Sci. Instrum.* **92**, 124502 (2021).
- [50] Representative uncertainties are related to electric field distribution, noise temperature measurements, and cavity parameters, see Ref. [33].
- [51] V. Anastassopoulos *et al.*, *Nat. Phys.* **13**, 584 (2017).
- [52] A. V. Dixit, S. Chakram, K. He, A. Agrawal, R. K. Naik, D. I. Schuster, and A. Chou, *Phys. Rev. Lett.* **126**, 141302 (2021).
- [53] M. Brune, S. Haroche, V. Lefevre, J. M. Raimond, and N. Zagury, *Phys. Rev. Lett.* **65**, 976 (1990).
- [54] A. Berlin, D. Blas, R. T. D’Agnolo, S. A. R. Ellis, R. Harnik, Y. Kahn, and J. Schütte-Engel, *Phys. Rev. D* **105**, 116011 (2022).
- [55] V. Domcke, C. Garcia-Cely, and N. L. Rodd, *Phys. Rev. Lett.* **129**, 041101 (2022).